



OPEN

# Weakening of the Atlantic Niño variability under global warming

Lander R. Crespo <sup>1,2</sup>, Arthur Prigent <sup>3</sup> ✉, Noel Keenlyside <sup>1,2,4</sup>, Shunya Koseki<sup>1,2</sup>, Lea Svendsen <sup>1,2</sup>, Ingo Richter <sup>5</sup> and Emilia Sánchez-Gómez<sup>6</sup>

**The Atlantic Niño is one of the most important patterns of interannual tropical climate variability, but how climate change will influence this pattern is not well known due to large climate model biases. Here we show that state-of-the-art climate models robustly predict a weakening of Atlantic Niños in response to global warming, mainly due to a decoupling of subsurface and surface temperature variations as the upper equatorial Atlantic Ocean warms. This weakening is predicted by most (>80%) models in the Coupled Model Intercomparison Project Phases 5 and 6 under the highest emission scenarios. Our results indicate a reduction in variability by the end of the century by 14%, and as much as 24–48% when accounting for model errors using a simple emergent constraint analysis. Such a weakening of Atlantic Niño variability will potentially impact climate conditions and the skill of seasonal predictions in many regions.**

The Atlantic Niño phenomenon exhibits many similarities to the stronger El Niño–Southern Oscillation<sup>1,2</sup> (ENSO) in the Pacific. The eastern equatorial Atlantic is anomalously warm, surface trade winds relax and rainfall shifts equatorward during positive Atlantic Niño<sup>3–6</sup> events. The sea surface temperature (SST) anomalies in the equatorial cold tongue can reach 1.5 °C, and thermocline (20 °C isotherm) depth anomalies can exceed 30 m in boreal summer when the events peak. Opposite conditions are found during negative events. Coupled ocean–atmosphere interactions—Bjerknes positive and delayed negative feedbacks—similar to those in the Pacific can explain most Atlantic Niño variability, but other mechanisms can contribute substantially to equatorial SST anomalies<sup>6,7</sup>. The Atlantic Niño has important impacts on the climate<sup>8–10</sup> and marine biogeochemistry<sup>11,12</sup> in the tropical Atlantic sector, on ENSO<sup>13–17</sup> and on extra-tropical climate<sup>18–21</sup>.

Recent studies have shown a weakening of the Atlantic Niño variability in the past decades<sup>22–24</sup>. The changes in eastern equatorial Atlantic SST variability have been attributed to the combined effect of a weakening of the Bjerknes feedback<sup>23</sup> (BF) and increased heat flux damping<sup>23,24</sup> and to a basin-wide warming related to climate change<sup>22</sup>. These studies used observational and reanalysis datasets to investigate changes in the SST variability during the historical period.

Extensive analysis of the projections from the Coupled Model Intercomparison Project (CMIP) indicates that ENSO events will become stronger under global warming, but large uncertainties exist<sup>25–30</sup>. Large climate model biases in the tropical Atlantic sector<sup>31–34</sup> have discouraged the climate community from carrying out a similar in-depth assessment of climate change in the area, as have the large uncertainties in the projected weakening of the Atlantic Meridional Overturning Circulation, in simulated Atlantic Multi-decadal Variability and in their influence on Atlantic Niño variability<sup>4</sup>. While robust shifts and weakening of Atlantic Niño teleconnections under future global warming have been identified<sup>21,35</sup>, large uncertainties exist in the local rainfall response to a potential

long-term weakening in Atlantic Niño variability<sup>36</sup>. However, we will show that model biases do not preclude a more robust assessment of global warming impacts on Atlantic Niño variability than has been achieved in the Pacific.

## Weakened variability of the equatorial Atlantic SST

To investigate how the SST variability in the eastern equatorial Atlantic will change under global warming, we use historical simulations and the future highest emissions scenario simulations from the CMIP5<sup>37</sup> and CMIP6<sup>38</sup> archives. The comparison between the historical (1950–1999) and the highest emissions future scenario (2050–2099) in the CMIP models shows that the SST variability in the eastern equatorial Atlantic sector in June, July and August (JJA) is reduced in the majority of the CMIP models (33 out of 40). The reduction is statistically significant at the 95% level in most of the models (23 out of 33) and there is no statistically significant increase in variability in any model (Supplementary Fig. 1, Fig. 1a and Supplementary Table 1). The multi-model ensemble mean of CMIP5 (CMIP6) shows a reduction of the SST variability of 12% (17%) in the future scenario simulation with respect to the historical simulation (Supplementary Table 1). Considering all CMIP5 and CMIP6 models, we have a most probable reduction of 14%, with an uncertainty of 17%.

The surface zonal winds (UAS, hereafter) in the western Atlantic sector also show a reduced future variability in the May, June and July (MJJ) season in the CMIP5 and CMIP6 models with only four out of 40 models showing increased variability, although not statistically significant (Supplementary Fig. 1, Fig. 1d and Supplementary Table 1). The reduction in SST and UAS variability across the CMIP models is field significant with global *P* values as small as 10<sup>–15</sup> and 10<sup>–11</sup>, respectively, which underscores the robustness of this finding (Methods). The standard deviation of the MJJ UAS anomalies averaged over the ensemble is reduced by 14% in CMIP5 and by 17% in CMIP6, consistent with the amplitude of the reduction in JJA SST variability (Supplementary Table 1). The reduction of the

<sup>1</sup>Geophysical Institute, University of Bergen, Bergen, Norway. <sup>2</sup>Bjerknes Centre for Climate Research, University of Bergen, Bergen, Norway. <sup>3</sup>GEOMAR Helmholtz Centre for Ocean Research Kiel, Kiel, Germany. <sup>4</sup>Nansen Environmental and Remote Sensing Centre, Bergen, Norway. <sup>5</sup>Japan Agency for Marine–Earth Science and Technology, JAMSTEC, Yokohama, Japan. <sup>6</sup>CECI, Université de Toulouse–Cerfacs–CNRS, Toulouse, France.

✉e-mail: [aprigent@geomar.de](mailto:aprigent@geomar.de)

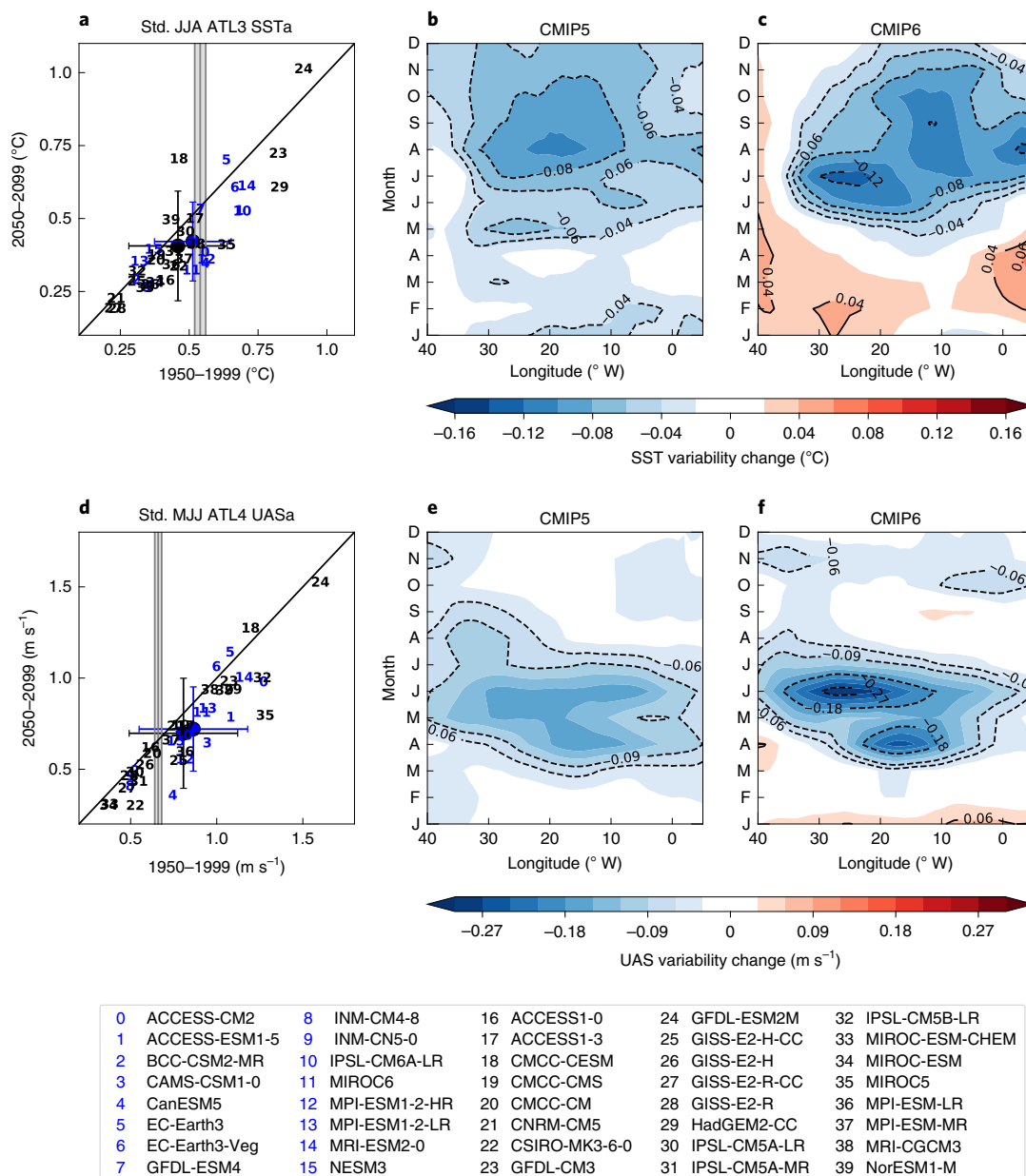


**Fig. 1 | Weakening of the eastern equatorial Atlantic SST variability.** **a**, Scatter plot of the JJA average standard deviation (Std.) of the SST anomalies (SSTa) for the historical period (1950–1999) in the x axis against the standard deviation of SSTa for the scenario period (2050–2099) in the y axis. The black line represents the no-change line and is added for easier interpretation. The blue (black) numbers correspond to the CMIP6 (CMIP5) models listed in Supplementary Table 1. The blue (black) circle shows the ensemble mean of CMIP6 (CMIP5) models. **b,c**, Difference between the means of the 2050–2099 and the 1950–1999 periods standard deviation of the SST anomalies for the ensemble mean of CMIP5 (**b**) and CMIP6 (**c**) models, along the equator and averaged between 3° S and 3° N. **d-f**, The same as **a-c** for the MJJ average standard deviation of the UASa. Grey vertical bars in **a** and **d** are observational estimates of the standard deviation of the ATL3-averaged JJA SSTa and ATL4-averaged MJJ UASa over the period 1982–2017. The grey shading is the  $\pm$  one standard deviation of the observational ensembles, composed of ERA5, ERSSTv5, OI-SST and HadISST for the SST and of ERA5, ERA-interim and NCEP-DOE Reanalysis 2 for the 10 m zonal winds. Months are identified by first letter in **b, c, e** and **f**. Contour lines in **b, c** and in **e, f** represent the change in SST variability and in UAS variability, respectively. Dashed (solid) contour lines indicate a reduction (increase) of the variability. Below the figure is a list of the CMIP6 and CMIP5 models used in this study.

UAS variability in the western equatorial Atlantic is consistent with a more stratified atmosphere in a future warmer climate<sup>35</sup>.

The reduction of the standard deviation in both SST and UAS is more pronounced and localized in the ensemble mean of CMIP6 (Fig. 1c,f) than in CMIP5 (Fig. 1b,e). The weakening of the standard deviation of the MJJ zonal winds in the western equatorial Atlantic is followed by a weakening of the eastern equatorial Atlantic JJA SST variability in both the CMIP5 (Fig. 1b,e)

and CMIP6 (Fig. 1c,f) ensemble means, suggesting that the reduced wind variability may be the cause of the reduced SST variability. However, the linear regression between the changes in these two variables across the ensemble of models explains only 33% of the variance (Supplementary Fig. 1). Consequently, there must be other mechanisms that play an important role in the reduction of the standard deviation of the SST in the eastern equatorial Atlantic.

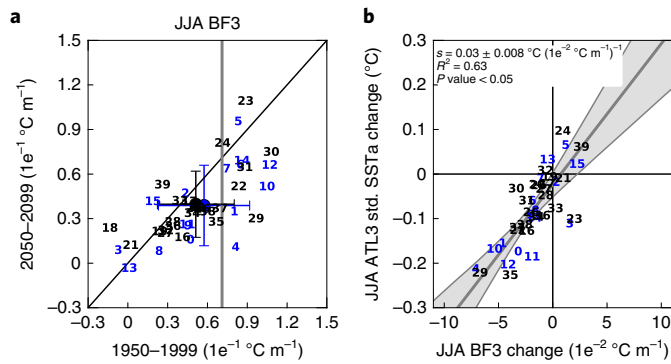


**Fig. 2 | Dynamical drivers of the weakening of the SST variability.**

**a**, Changes between the historical and future scenario in the strength of the third component of the BF, computed as the linear regression of ATL3 JJA SSTA onto the ATL3 JJA 20 °C isotherm depth (Z20) anomalies. The blue and black dots are the ensemble means of the CMIP6 and CMIP5 ensemble, respectively. **b**, Linear regression between the change in JJA SSTA standard deviation and the change in the third BF component. The change here is defined as the difference of the mean of the scenario period (2050–2099) minus the mean of the historical period (1950–1999). The vertical grey line in **a** represents an estimation of the third component of the BF from observation and reanalysis datasets over the period 1982–2017. The grey shading depicts the 95% confidence interval of the linear regression. The confidence interval is obtained by taking the 2.5th and 97.5th percentile of the distribution of the linear regressions of the 10,000-time resampled datasets. The blue (black) numbers correspond to the CMIP6 (CMIP5) models listed in Supplementary Table 1.

### Weakened ocean–atmosphere coupling

We explore the relative importance of the dynamical and thermodynamical drivers of the future changes in the SST, through the BF components and the net heat flux damping (Methods). The basin-wide weakening of the SST variability and winds in the future scenario simulation might be related to a weakening of the BF. As the changes in variability in CMIP5 and CMIP6 are rather similar, we will consider all CMIP models together in this section.

A majority of the CMIP models, 29 out of 40, agree on a small decrease of the first component of the BF; that is the linear regression of MJJ ATL4 zonal winds anomalies on the JJA ATL3 sea surface temperature anomalies (SSTA) (Supplementary Fig. 2a). The second component of the BF, the thermocline zonal slope response to western equatorial wind anomalies, is reduced in 26 out of 40 models, but the overall decrease is small (Supplementary Fig. 2b). The third component of the BF, which accounts for the local response of SSTA to thermocline depth anomalies in the ATL3 region, shows the most consistent changes among the models, with 30 out of 40 CMIP models showing a reduction of the third BF component (Fig. 2a). Both the CMIP5 and the CMIP6 multi-model ensemble means show a reduction in the strength of this relation in the future climate simulations (Fig. 2a).

There is a strong relation between changes in ATL3 JJA SSTA variability and the strength of the third BF component that explains 63% of the spread across the CMIP models (Fig. 2b). Contrastingly, the changes in the first and second components of the BF explain only little variance of the change in SST variability, 20% and 19% (Supplementary Fig. 2c,d). Therefore, the reduced sensitivity of SST to local changes in thermocline depth dominates the reduction of SST variability in the eastern equatorial Atlantic in the future scenario. The relevance of the thermocline feedback for the reduced variability of Atlantic Niño in recent decades has also been observed<sup>22</sup>. However, the majority of the CMIP models largely underestimates the strength of this part of the feedback in historical

simulations (Fig. 2a), a flaw already present in CMIP5 models<sup>39</sup> that still persists in the latest CMIP6 generation. As shown below, this causes an overall underestimation of the future reduction of SST variability by the CMIP models. Nevertheless, we are confident in using these models to investigate climate change impacts on the Atlantic Niño, as they do simulate the essential dynamics of this phenomenon<sup>4,34</sup> (Fig. 2a and Supplementary Fig. 2a,b).

### Future mean changes of the tropical Atlantic SST

The strength of the third component of the BF, known as the thermocline feedback, is linked to the strength of climatological upwelling and vertical temperature stratification<sup>40</sup>. In particular, a weaker feedback can result from the weaker upwelling of relatively warmer subsurface waters. Despite a large intermodel spread, the SST change between historical and future scenario simulations shows a robust warming of the equatorial Atlantic cold tongue consistent with a weakening of the third BF component (Supplementary Table 1). The future scenario simulations of CMIP5 and CMIP6 models present a warming (Supplementary Table 1) of the JJA in the eastern equatorial Atlantic of  $2.70 \pm 0.58$  °C and  $2.54 \pm 0.79$  °C, respectively. The CMIP5 and CMIP6 ensembles show a mean warming of 2 °C to 3 °C in the tropical Atlantic sector between the historical and the future scenario simulations (Fig. 3a,b). The spatial patterns of the future warming rate in the multi-model ensemble mean of both CMIPs are rather similar and show a strong zonally homogeneous warming along the equatorial band. The trade winds are projected to weaken in most of the tropical Atlantic in CMIP5 and CMIP6, coinciding with the warming pattern (Fig. 3a,b). In the CMIP6 ensemble mean, the weakening of the trade winds is particularly strong in the eastern equatorial Atlantic and north of 10° N (Fig. 3b). Weaker equatorial trade winds will weaken equatorial upwelling and thereby contribute to a weaker third component of the BF.

The vertical section along the equatorial Atlantic clearly shows that future warming of the upper ocean will be greatest from the surface down to about 50 m in the eastern equatorial Atlantic and 70 m in the western equatorial Atlantic in the CMIP5 ensemble mean (Fig. 3c). The warming of the upper levels is rather zonally homogeneous in both CMIP5 and CMIP6. However, this is not the case for the deeper levels where the eastern equatorial Atlantic is warming faster than the western side of the basin; this warming pattern could be related to changes in oceanic circulation associated with the subtropical cells and Atlantic Meridional Overturning Circulation<sup>41</sup>. The strong warming of the upper levels in the ensemble mean of both CMIP generations leads to a deeper thermocline in the future scenario (Fig. 3c,d). As the thermocline gets deeper, the coupling between the thermocline and the SST weakens<sup>42</sup>. In other words, the variability in the SST is less sensitive to the variability of the thermocline, in agreement with the previously shown weakening of the third component of the BF (Fig. 2b). The reduction of the SST variability could also be affected by changes in the thermodynamical coupling between the ocean and the atmosphere. However, we find that in the CMIP models, the thermodynamical mechanism is not relevant for explaining the change in the SST variance between the future climate and the historical climate periods (Supplementary Fig. 3).

### Impact of model biases

Coupled general circulation models show large biases in the tropical Atlantic region<sup>31–34,43,44</sup> and, in particular, a warm SST bias in JJA in the eastern equatorial Atlantic, where projected changes in SST variability are largest. We find that the models with smaller bias have a stronger reduction in SST variability (Fig. 4a), a stronger reduction in the third BF component (that is, the thermocline feedback) (Fig. 4b) and a larger SST change between future scenario and historical (Fig. 4c). Therefore, biases in the models seem to suppress the reduction of

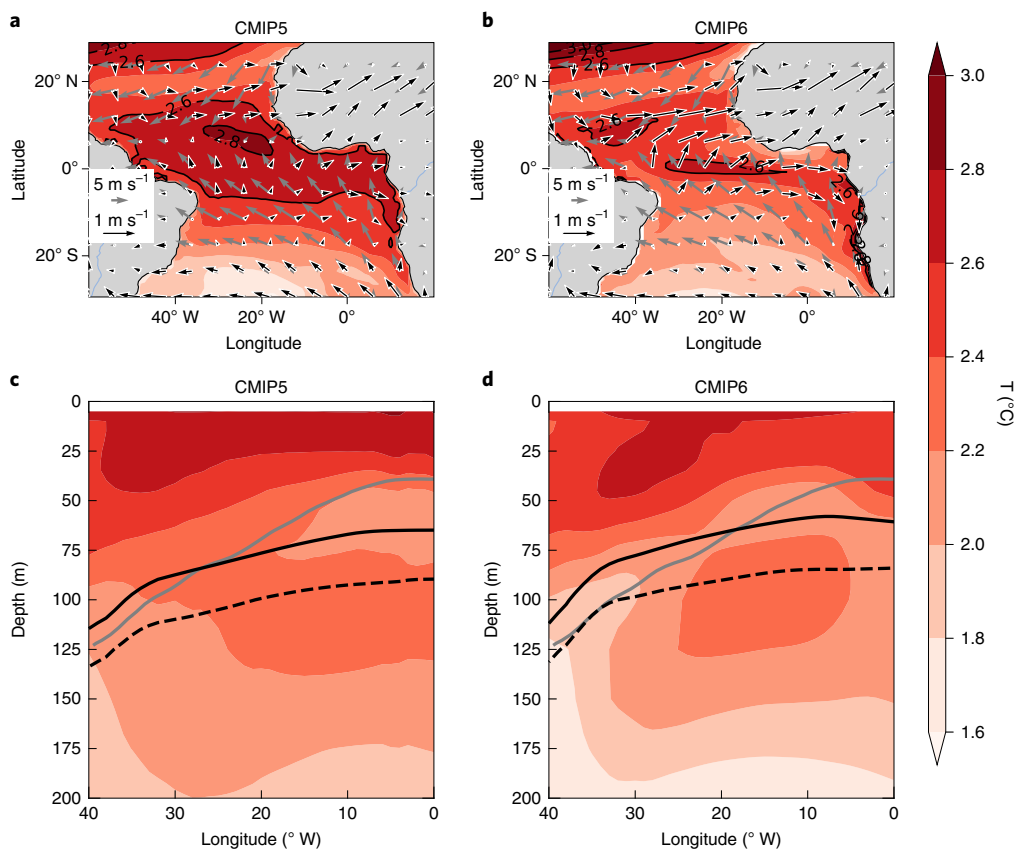


**Fig. 3 | Mean state changes in the equatorial Atlantic. a, b,** Difference between future scenario and historical simulations of JJA SST (in shading) and JJA surface winds (black arrows) for the multi-model ensemble means of CMIP5 (**a**) and CMIP6 (**b**). The grey arrows depict the mean historical surface winds. The units are  $^{\circ}\text{C}$  and  $\text{m s}^{-1}$  for SST and for surface winds, respectively. **c, d,** Vertical section of the difference in ocean temperature between future scenario and historical simulations for CMIP5 (**c**) and CMIP6 (**d**) multi-model ensemble means for JJA average. The black solid (dashed) line represents the depth of the  $20^{\circ}\text{C}$  isotherm for the climatological mean of the historical (future scenario) period. The temperature has been latitudinally averaged from  $3^{\circ}\text{S}$  to  $3^{\circ}\text{N}$ . The periods taken for the historical and the future scenario simulations are 1950–1999 and 2050–2099, respectively. The grey lines in **c** and **d** represent the JJA ORA-S4  $20^{\circ}\text{C}$  isotherm depth over the period 1982–2017.

the SST variability in a future warmer climate through a reduction of the weakening of the thermocline feedback.

This relation with SST bias is expected. The strength of the equatorial cold tongue and the thermocline feedback are connected through the intensity of equatorial upwelling and upper ocean vertical temperature gradients. Thereby, a stronger cold tongue is associated with a stronger thermocline feedback (explained variance of 28%, Fig. 4b) and shallower thermocline<sup>4</sup>. Additionally, models with a stronger cold tongue (that is, less biased) show a stronger weakening of the cold tongue through a stronger weakening of the thermocline feedback (explained variances of 19% and 28%, Fig. 4c,d); supporting previous studies linking the cold tongue bias and SST changes<sup>45,46</sup>. However, SST biases and changes in SST variability are not simply related to the thermocline depth biases (Supplementary Fig. 4a), although in most models, the eastern equatorial thermocline is too deep (Fig. 3c,d) and equatorial SST too warm (Supplementary Fig. 4b).

An emergent constraint analysis can be used to better estimate future changes when robust mechanisms exist<sup>47</sup>. These statistically significant and physically based relationships identify the strength of the Atlantic cold tongue as an emergent constraint for changes in Atlantic Niño variability (Methods). In particular, the cold tongue SST bias and changes in SST variability present a physically robust relation that explains almost 27% of the variance across the models (Fig. 4a). This emergent relation indicates that a reduction of

$0.18^{\circ}\text{C}$  in the standard deviation is most realistic, with a range of  $0.13$ – $0.26^{\circ}\text{C}$  determined by uncertainties in the linear regression relation. The standard deviation of the observed ATL3-averaged JJA SSTa variability is about  $0.54^{\circ}\text{C}$  during the period 1982–2017. Thus, accounting for model errors implies a reduction in variability of around 33%, with a range of 24–48% that is much larger than the  $14 \pm 17\%$  predicted when considering all models (Supplementary Table 1).

### Concluding remarks

Eastern equatorial Atlantic SST variability is projected to weaken under global warming following the future highest emission scenario simulations of the CMIP5 and CMIP6 models. Similarly, the variability of the zonal surface wind in the western equatorial Atlantic will also weaken and is related to the reduction in SST variability as it explains 33% of the intermodel variance, but it is not the exclusive reason. Instead, changes in the strength of ocean–atmosphere interaction drive the weaker SST variability. The weakening of the third component of the BE, the so-called thermocline feedback, explains 63% of the change in the SST variability, independent of the change in surface wind variability.

We find that in a warmer future climate, the upper ocean layer will become deeper, which makes it less sensitive to upwelling anomalies, and equatorial trade winds weaken, which reduces mean upwelling strength and thus the impact of subsurface temperature



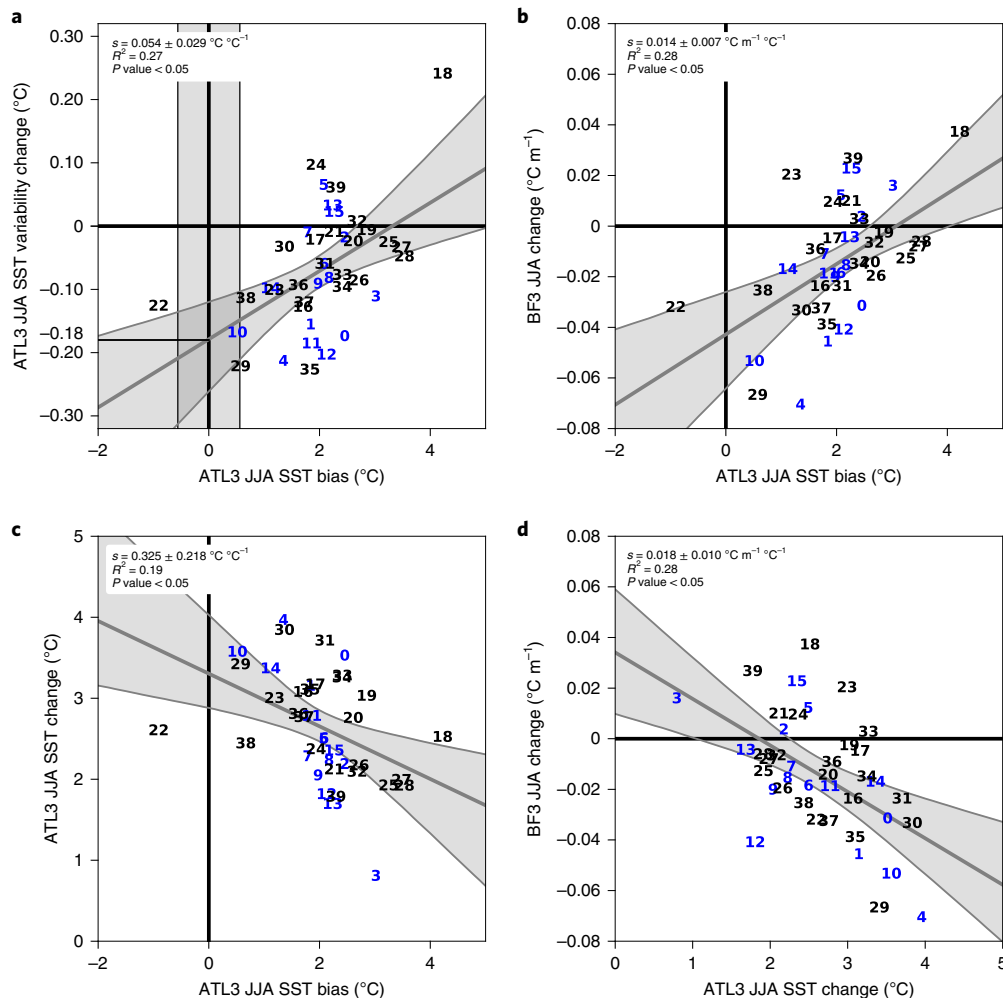


**Fig. 4 | Impact of model biases.** **a**, Scatter plot of the JJA ATL3-averaged SST bias and SST variability change. The SST bias is estimated as the difference between detrended model SST and detrended HadISST over the period 1950–1999. The grey shading around  $0 \text{ } ^\circ\text{C}$  bias is  $\pm$  the standard deviation of the detrended ATL3-averaged JJA HadISST over the period 1950–1999. **b**, Scatter plot of JJA ATL3-averaged SST bias and BF3 change. **c**, Scatter plot of JJA ATL3-averaged SST bias and mean SST change. **d**, Scatter plot of JJA ATL3-averaged mean SST change and BF3 change. The change here is defined as the difference of the mean of the scenario period (2050–2099) minus the mean of the historical period (1950–1999). The grey shading depicts the 95% confidence interval of the linear regression. The confidence interval is obtained by taking the 2.5th and 97.5th percentile of the distribution of the linear regressions of the 10,000-time resampled datasets. The blue (black) numbers correspond to the CMIP6 (CMIP5) models listed in Supplementary Table 1.

anomalies. This together leads to a weakening of the thermocline feedback because the thermocline decouples from the SST variability. This mechanism is remarkably different from the driving mechanisms of climate change in the equatorial Pacific, where the changes in the zonal SST gradient under greenhouse forcing are most relevant<sup>26,48</sup>. However, in contrast to our findings in the Atlantic, the models in the Pacific show little agreement on the sign of the change in SST gradient<sup>48</sup>.

The future weakening of the boreal summer SST variability in the eastern equatorial Atlantic shows large agreement across model ensembles of both CMIP generations. Moreover, the weakening of SST variability is found in the multi-model ensemble mean of the most commonly considered future scenarios (Supplementary Figs. 5 and 6) and in the majority of the individual models. Furthermore, although biased, many models simulate key aspects of the Atlantic Niño, including the BF. Therefore, we are confident in the robustness of our results.

The reduction of the SST variability in the future climate could be interpreted as an amplification of the already observed weakening in the recent decades that has been attributed to a weakening of

the BF and a stronger thermal damping<sup>22–24</sup>. The role of the BF in the CMIP models is key for the weakening in SST variability. On the other hand, the CMIP models do not show a significant relationship between changes in the surface net heat fluxes and changes in the SST variability. Furthermore, the models do not reproduce the strong reduction of SST variability in recent decades, simulating a gradual and up to 20 times smaller decrease of the interannual SST variability (Supplementary Table 2). This discrepancy with observations could be caused by internal climate variability or by model error and exists even considering the exceptionally strong 2019<sup>49</sup> and 2021 Atlantic Niño events.

We find that the future weakening is stronger in the models with smaller SST biases. The amplitude of the projected SST variability is closely related to the strength of the CMIP model biases through a physically consistent mechanism. This emergent constraint predicts a most likely variability reduction of around 33%. Thus, reducing the biases in the models should increase the reliability of the climate projections in the tropical Atlantic sector and greatly improve our assessment of climate change in the region. We expect the reduced SST variability to have important climate impacts locally

and globally, and current and future research should focus on the impacts on rainfall<sup>36</sup>, on marine productivity and on changes in the atmospheric circulation among others.

### Online content

Any methods, additional references, Nature Research reporting summaries, source data, extended data, supplementary information, acknowledgements, peer review information; details of author contributions and competing interests; and statements of data and code availability are available at <https://doi.org/10.1038/s41558-022-01453-y>.

Received: 6 May 2022; Accepted: 19 July 2022;

Published online: 1 September 2022

### References

- McPhaden, M. J., Zebiak, S. E. & Glantz, M. H. ENSO as an integrating concept in Earth science. *Science* **314**, 1740–1745 (2006).
- Timmermann, A. et al. El Niño–Southern Oscillation complexity. *Nature* **559**, 535–545 (2018).
- Keenlyside, N. & Latif, M. Understanding equatorial Atlantic interannual variability. *J. Clim.* **20**, 131–142 (2007).
- Lübbecke, J. F. et al. Equatorial Atlantic variability—Modes, mechanisms, and global teleconnections. *Wiley Interdiscip. Rev. Clim. Change* **9**, e527 (2018).
- Zebiak, S. Air–sea interaction in the equatorial Atlantic region. *J. Clim.* **6**, 1567–1586 (1993).
- Richter, I. & Tokinaga, H. in *Tropical and Extratropical Air–Sea Interactions* (ed. Behera, S. K.) Ch. 7 (Elsevier, 2021).
- Richter, I. et al. Multiple causes of interannual sea surface temperature variability in the equatorial Atlantic Ocean. *Nat. Geosci.* **6**, 43–47 (2013).
- Hirst, A. & Hastenrath, S. Atmosphere–ocean mechanisms of climate anomalies in the Angola–Tropical Atlantic sector. *J. Phys. Oceanogr.* **13**, 1146–1157 (1983).
- Nobre, P. & Shukla, J. Variations of SST, wind stress and rainfall over the tropical Atlantic and South America. *J. Clim.* **9**, 2464–2479 (1996).
- Gu, G. & Adler, R. Seasonal evolution and variability associated with the West African monsoon system. *J. Clim.* **17**, 3364–3377 (2004).
- Boyd, A., Tauntonclark, J. & Oberholster, G. Spatial features of the near-surface and midwater circulation patterns off western and southern South Africa and their role in the life histories of various commercially fished species. *S. Afr. J. Mar. Sci.* **12**, 189206 (1992).
- Chenillat, F. et al. How do climate modes shape the chlorophyll-a interannual variability in the tropical Atlantic? *Geophys. Res. Lett.* **48**, e2021GL093769 (2021).
- Rodríguez-Fonseca, B. et al. Are Atlantic Niños enhancing Pacific ENSO events in recent decades? *Geophys. Res. Lett.* **36**, L20705 (2009).
- Ding, H., Keenlyside, N. & Latif, M. Impact of the equatorial Atlantic on the El Niño Southern Oscillation. *Clim. Dynam.* **38**, 1965–1972 (2012).
- Polo, I., Martín-Rey, M., Rodríguez-Fonseca, B., Kucharski, F. & Mechoso, C. Processes in the Pacific La Niña onset triggered by the Atlantic Niño. *Clim. Dyn.* **44**, 115–131 (2015).
- Martín-Rey, M., Rodríguez-Fonseca, B. & Polo, I. Atlantic opportunities for ENSO prediction. *Geophys. Res. Lett.* **42**, 6802–6810 (2015).
- Exarchou, E. et al. Impact of equatorial Atlantic variability on ENSO predictive skill. *Nat. Commun.* **12**, 1612 (2021).
- García-Serrano, J., Losada, T., Rodríguez-Fonseca, B. & Polo, I. Tropical Atlantic variability modes (1979–2002). Part II: time-evolving atmospheric circulation related to SST-forced tropical convection. *J. Clim.* **21**, 6476–6497 (2008).
- Haarsma, R. J. & Hazeleger, W. Extratropical atmospheric response to equatorial Atlantic cold tongue anomalies. *J. Clim.* **20**, 2076–2091 (2007).
- Losada, T., Rodríguez-Fonseca, B. & Kucharski, F. Tropical influence on the summer Mediterranean climate. *Atmos. Sci. Lett.* **13**, 36–42 (2012).
- Mohino, E. & Losada, T. Impacts of the Atlantic equatorial mode in a warmer climate. *Clim. Dyn.* **45**, 2255–2271 (2015).
- Tokinaga, H. & Xie, S. P. Weakening of the equatorial Atlantic cold tongue over the past six decades. *Nat. Geosci.* **4**, 222–226 (2011).
- Prigent, A., Lübbecke, J., Bayr, T., Latif, M. & Wengel, C. Weakened SST variability in the tropical Atlantic Ocean since 2000. *Clim. Dyn.* **54**, 2731–2744 (2020).
- Silva, P., Wainer, I. & Khodri, M. Changes in the equatorial mode of the Tropical Atlantic in terms of the Bjerknes Feedback Index. *Clim. Dyn.* <https://doi.org/10.1007/s00382-021-05627-w> (2021).
- Lübbecke, J. & McPhaden, M. J. Assessing the twenty-first century shift in ENSO variability in terms of the Bjerknes stability index. *J. Clim.* **27**, 2577–2587 (2014).
- Collins, M. et al. The impact of global warming on the tropical Pacific Ocean and El Niño. *Nat. Geosci.* **3**, 391–397 (2010).
- DiNezio, P. N. et al. Mean climate controls on the simulated response of ENSO to increasing greenhouse gases. *J. Clim.* **25**, 7399–7420 (2012).
- Kim, S. et al. Response of El Niño sea surface temperature variability to greenhouse warming. *Nat. Clim. Change* **4**, 786–790 (2014).
- Cai, W. et al. Increasing frequency of extreme El Niño events due to greenhouse warming. *Nat. Clim. Change* **4**, 111–116 (2014).
- Cai, W. et al. Increased frequency of extreme La Niña events under greenhouse warming. *Nat. Clim. Change* **5**, 132–137 (2015).
- Li, G. & Xie, S. P. Origins of tropical-wide SST biases in CMIP multi-model ensembles. *Geophys. Res. Lett.* **39**, L22703 (2012).
- Richter, I., Xie, S. P., Behera, S. K., Doi, T. & Masumoto, Y. Equatorial Atlantic variability and its relation to mean state biases in CMIP5. *Clim. Dyn.* **42**, 171–188 (2014).
- Richter, I., Xie, S. P., Wittenberg, A. T. & Masumoto, Y. Tropical Atlantic biases and their relation to surface wind stress and terrestrial precipitation. *Clim. Dyn.* **38**, 985–1001 (2012).
- Richter, I. & Tokinaga, H. An overview of the performance of CMIP6 models in the tropical Atlantic: mean state, variability, and remote impacts. *Clim. Dyn.* **55**, 2579–2601 (2020).
- Jia, F. et al. Weakening Atlantic Niño–Pacific connection under greenhouse warming. *Sci. Adv.* **5**, eaax4111 (2019).
- Worou, K., Goosse, H., Fichet, T. & Kucharski, F. Weakened impact of the Atlantic Niño on the future equatorial Atlantic and Guinea Coast rainfall. *Earth Syst. Dynam.* **13**, 231–249 (2022).
- Taylor, K. E., Stouffer, R. J. & Meehl, G. A. An overview of CMIP5 and the experiment design. *Bull. Am. Meteorol. Soc.* **93**, 485–498 (2012).
- Eyring, V. et al. Overview of the Coupled Model Intercomparison Project Phase 6 (CMIP6) experimental design and organisation. *Geosci. Model Dev.* **8**, 10539–10583 (2015).
- Deppenmeier, A. L., Haarsma, R. J. & Hazeleger, W. The Bjerknes feedback in the tropical Atlantic in CMIP5 models. *Clim. Dyn.* **47**, 2691–2707 (2016).
- Ding, H., Keenlyside, N., Latif, M., Park, W. & Wahl, S. The impact of mean state errors on equatorial Atlantic interannual variability in a climate model. *J. Geophys. Res. Oceans* **120**, 1133–1151 (2015).
- Chang, P. et al. Oceanic link between abrupt changes in the North Atlantic Ocean and the African monsoon. *Nat. Geosci.* **1**, 444–448 (2008).
- Zebiak, S. E. & Cane, M. A. A model El Niño–Southern Oscillation. *Mon. Weather Rev.* **115**, 2262–2278 (1987).
- Exarchou, E. et al. Origin of the warm eastern tropical Atlantic SST bias in a climate model. *Clim. Dyn.* **51**, 1819–1840 (2018).
- Voldoire, A. et al. Role of wind stress in driving SST biases in the tropical Atlantic. *Clim. Dyn.* **53**, 3481–3504 (2019).
- Park, W. & Latif, M. Resolution dependence of CO<sub>2</sub>-induced tropical Atlantic sector climate changes. *npj Clim. Atmos. Sci.* **3**, 36 (2020).
- Imbol Nkwinkwa, A. S. N., Latif, M. & Park, W. Mean-state dependence of CO<sub>2</sub>-forced tropical Atlantic sector climate change. *Geophys. Res. Lett.* **48**, e2021GL093803 (2021).
- Hall, A. & Qu, X. Using the current seasonal cycle to constrain snow albedo feedback in future climate change. *Geophys. Res. Lett.* **33**, L03502 (2006).
- Heede, U. K., Fedorov, A. V. & Burls, N. J. A stronger versus weaker Walker: understanding model differences in fast and slow tropical Pacific responses to global warming. *Clim. Dyn.* <https://doi.org/10.1007/s00382-021-05818-5> (2021).
- Richter, I., Tokinaga, H. & Okumura, Y. M. The extraordinary equatorial Atlantic warming in late 2019. *Geophys. Res. Lett.* **49**, e2021GL095918 (2022).

**Publisher's note** Springer Nature remains neutral with regard to jurisdictional claims in published maps and institutional affiliations.



**Open Access** This article is licensed under a Creative Commons Attribution 4.0 International License, which permits use, sharing, adaptation, distribution and reproduction in any medium or format, as long as you give appropriate credit to the original author(s) and the source, provide a link to the Creative Commons license, and indicate if changes were made. The images or other third party material in this article are included in the article's Creative Commons license, unless indicated otherwise in a credit line to the material. If material is not included in the article's Creative Commons license and your intended use is not permitted by statutory regulation or exceeds the permitted use, you will need to obtain permission directly from the copyright holder. To view a copy of this license, visit <http://creativecommons.org/licenses/by/4.0/>.

© The Author(s) 2022

## Methods

**Data.** We use monthly mean model output obtained from the two latest CMIP generations: CMIP5 (ref. <sup>37</sup>) and CMIP6 (ref. <sup>38</sup>). We use the following fields from the CMIP models: SST, UAS, surface heat fluxes and ocean potential temperature. The latter is used to derive the depth of the 20°C isotherm depth, which serves as a proxy for thermocline depth (Z20, hereafter). We use the Hadley Centre Sea Ice and Sea Surface Temperature dataset (HadISST)<sup>50</sup> to compute the model SST biases over the period 1950–1999. We also use an ensemble composed of the European Centre for Medium-range Weather forecast (ECMWF) Re-Analysis version 5 (ERA5)<sup>51</sup>, the NOAA Extended Reconstructed Sea Surface Temperature version 5 (ERSSTv5)<sup>52</sup>, the HadISST and the Optimum Interpolation SST analysis version 2 (OISSTv2)<sup>53</sup> to estimate the ATL3-averaged JJA SST variability over the period 1982–2017. We use an ensemble composed of ERA5, ECMWF Re-Analysis (ERA-interim)<sup>54</sup> and the NCEP-DOE Reanalysis 2<sup>55</sup> to estimate the ATL4-averaged MJJ 10 m zonal wind variability over the period 1982–2017. In addition, we use (OI-SST)<sup>56</sup> available at 1° by 1° horizontal resolution for the period 1981/12 to 2019/12; the temperature from Ocean Reanalysis System Version 4 (ORA-S4)<sup>57</sup> from the European Centre for Medium-range Weather forecast (ECMWF) available at 1° by 1° horizontal resolution for the period 1958/01 to 2017/12; and the zonal wind speed ERA-interim<sup>54</sup> available at 0.5° by 0.5° horizontal resolution for the period 1979/01 to 2018/12 to estimate the three components of the BF over the period 1982/01–2017/12. We investigate future climate changes in the equatorial Atlantic using the future emission scenarios, RCP26, RCP45, RCP60, RCP85 and SSP126, SSP245, SSP370, SSP585, for CMIP5 and CMIP6, respectively. However, most of our results are based on the comparison between historical simulation and the highest emissions scenario simulations RCP85 and SSP585. The climate models used in this study are listed in Fig. 1 and Supplementary Table 1. We use one ensemble member for each of the models, and all model data have been interpolated to a common horizontal 1° × 1° grid.

**Statistical metrics.** We use the standard deviation of the JJA SSTa and the MJJ UASa as metrics to investigate the changes in variability between the simulated historical and future climate periods. The season JJA (MJJ) is chosen for the SST (UAS) variability as it is the season of largest SST (UAS) variability in CMIP5 and CMIP6 models. For this analysis we use the 50-year periods January 1950 to December 1999 and January 2050 to December 2099 for the historical and scenario simulations, respectively. We calculate the monthly anomalies by subtracting the seasonal cycle evaluated for each time period. All linear trends are removed before analysis.

**Statistical significance.** The evaluation of the statistical significance of variability changes in a single model is based on an F-test. Additionally, we compute the group significance of two of our main findings: the projected reductions of the variability in SST and UAS. The group significance<sup>58</sup> is computed using two different methods: (i) the Livezey–Chen<sup>59</sup> procedure that checks for group significance based on the binomial distribution function. This method consists of counting the number of local tests that are significant. The global null hypothesis can be rejected if the probability of having obtained the observed number of local test rejections is not larger than the chosen global *P* value. This probability is computed from the binomial probability distribution function that takes as input the number of occurrences, the successes and the *P* value of choice. (ii) the Benjamini–Hochberg procedure<sup>60</sup> that corrects the local *P* values using the False Discovery Rate method which accounts for potential false rejections of the null hypothesis. The global null hypothesis implies that all local null hypotheses are accepted. The individual local null hypothesis can be rejected if the corrected *P* value is smaller than the False Discovery Rate (set to 0.05 in our case). If one or more of the local null hypotheses is rejected, then we can reject the global null hypothesis and state that our statistics are group or field significant<sup>58</sup> at the 95% significance level.

**Quantification of dynamical ocean–atmosphere feedbacks.** We compute the three components of the BF that involve SST, thermocline depth and zonal surface winds<sup>61</sup> to explore the potential dynamical drivers of the future changes in SST variability. The three components of the BF are estimated through linear regression of (1) western equatorial Atlantic (3°S–3°N, 40°W–20°W; ATL4) zonal wind stress anomalies upon eastern equatorial Atlantic (3°S–3°N, 20°W–0°; ATL3) SST anomalies, (2) equatorial thermocline slope anomalies regressed onto ATL4 zonal wind stress anomalies and (3) SSTa in ATL3 upon thermocline depth anomalies in ATL3. The equatorial thermocline slope is computed as the difference between the mean Z20 in ATL3 and ATL4. Linear ordinary least squares regressions are used to perform the linear regression in this study. The two-sided 95% confidence interval of the regression slopes is based on a Student's *t*-distribution.

**Emergent constraint analysis.** We perform an emergent constraint analysis to explore the impact of model biases on our findings. We use the SST bias in the JJA season during the historical period as our constraint. The SST bias is estimated as the difference between detrended model SST and detrended

HadISST over the period 1950–1999. The grey shading around 0°C bias is  $\pm$  the standard deviation of the detrended ATL3-averaged JJA mean HadISST over the period 1950–1999. The intersection between the linear regression of the ATL3-averaged JJA SST variability changes onto the SST bias, and the 0°C bias gives an indication on the potential reduction of the ATL3-averaged JJA SST variability if there were no SST bias in the CMIP models.

## Data availability

The CMIP6 data can be found at <https://esgf-data.dkrz.de/search/cmip6-dkrz/>. The CMIP5 data can be found at <https://esgf-node.llnl.gov/search/cmip5/>. The ERA5 data can be found at <https://cds.climate.copernicus.eu/cdsapp#!dataset/reanalysis-era5-single-levels-monthly-means?tab=form>. The ERSSTv5 data can be found at <https://psl.noaa.gov/data/gridded/data.noaa.ersst.v5.html>. The OI-SST data can be found at <https://psl.noaa.gov/data/gridded/data.noaa.oisst.v2.highres.html>. The HadISST data can be found at <https://www.metoffice.gov.uk/hadobs/hadisst/>. The NCEP-DOE Reanalysis 2 data can be found at <https://psl.noaa.gov/data/gridded/data.ncep.reanalysis2.html>. The ORA-S4 data can be found at <https://www.cen.uni-hamburg.de/en/icdc/data/ocean/easy-init-ocean/ecmwf-ocean-reanalysis-system-4-oras4.html> and the ERA-interim data can be found at <https://www.ecmwf.int/en/forecasts/datasets/reanalysis-datasets/era-interim>.

## Code availability

The data analysis was conducted using the software CDO (<https://code.mpimet.mpg.de/projects/cdo/embedded/cdo.pdf>), Matlab (<https://www.mathworks.com/products/matlab.html>) and Python (<https://www.python.org/>). The code that was used for data processing, model analysis and figure production is available at <https://doi.org/10.5281/zenodo.6815433>.

## References

- Rayner, N. A. et al. Global analyses of sea surface temperature, sea ice, and night marine air temperature since the late nineteenth century. *J. Geophys. Res.* **108**, 4407 (2003).
- Hersbach, H. et al. The ERA5 global reanalysis. *Q. J. R. Meteorol. Soc.* **146**, 1999–2049 (2020).
- Huang, B. et al. Extended Reconstructed Sea Surface Temperature version 5 (ERSSTv5), upgrades, validations, and intercomparisons. *J. Clim.* <https://doi.org/10.1175/JCLI-D-16-0836.1> (2017).
- Huang, B. et al. Improvements of the Daily Optimum Interpolation Sea Surface Temperature (DOISST) version 2.1. *J. Clim.* **34**, 2923–2939 (2021).
- Dee, D. P. et al. The ERA-Interim reanalysis: configuration and performance of the data assimilation system. *Q. J. R. Meteorol. Soc.* **137**, 553–597 (2011).
- Kanamitsu, M. et al. NCEP-DOE AMIP-II reanalysis (R-2). *Bull. Am. Meteorol. Soc.* **83**, 1631–1643 (2002).
- Reynolds, R. W. et al. Daily high-resolution-blended analyses for sea surface temperature. *J. Clim.* **20**, 5473–5496 (2007).
- Balmaseda, M. A., Mogensen, K. & Weaver, A. T. Evaluation of the ECMWF ocean reanalysis system ORAS4. *Q. J. R. Meteorol. Soc.* **139**, 1132–1161 (2013).
- Wilks, D. S. On “field significance” and the false discovery rate. *J. Appl. Meteorol. Climatol.* **45**, 1181–1189 (2006).
- Livezey, R. E. & Chen, W. Y. Statistical field significance and its determination by Monte-Carlo techniques. *Mon. Weather Rev.* **111**, 46–59 (1983).
- Benjamini, Y. & Hochberg, Y. Controlling the false discovery rate: a practical and powerful approach to multiple testing. *J. R. Stat. Soc. B* **57**, 289–300 (1995).
- Lübbecke, J. F. & McPhaden, M. J. Symmetry of the Atlantic Niño mode. *Geophys. Res. Lett.* **44**, 965–973 (2017).
- Crespo, L. R. et al. Scripts: weakening of the Atlantic Niño variability under global warming. *Zenodo* <https://doi.org/10.5281/zenodo.6815433> (2022).

## Acknowledgements

This study was supported by the TRIATLAS project funded under European Union's Horizon 2020 programme (grant agreement number 817578; L.R.C., N.K., S.K., E.S.-G.); and by the Bjerknes Climate Prediction Unit with funding from the Trond Mohn Foundation (grant BFS2018TMT01; N.K., L.S.). This study was partially supported by the German Federal Ministry of Education and Research as part of the BANINO project (03F0795A; A.P.). We also acknowledge Norwegian national computing and storage resources provided by UNINETT Sigma2 AS (NN9039K, NS9039K).

## Author contributions

N.K. initiated the study. L.R.C., N.K., S.K., I.R., L.S. and E.S.-G. designed the research. L.R.C. and A.P. performed all the analysis and prepared the figures. L.R.C. and A.P. wrote the first draft. All authors read and commented on the text.

**Funding**

Open access funding provided by GEOMAR Helmholtz-Zentrum für Ozeanforschung Kiel. The research was supported by the TRIATLAS project, which has received funding from the European Union's Horizon 2020 research and innovation programme under grant agreement No 817578.

**Competing interests**

The authors declare no competing interests.

**Additional information**

**Supplementary information** The online version contains supplementary material available at <https://doi.org/10.1038/s41558-022-01453-y>.

**Correspondence and requests for materials** should be addressed to Arthur Prigent.

**Peer review information** *Nature Climate Change* thanks Sergey Gulev and the other, anonymous, reviewer(s) for their contribution to the peer review of this work.

**Reprints and permissions information** is available at [www.nature.com/reprints](http://www.nature.com/reprints).